Net energy-oriented agitation optimization for cow manure–corn straw co-fermentation

Yuyingnan Liu[1], Kejia Zhang[1], Yong Sun[1,2*]

(1. *College of Engineering, Northeast Agricultural University, Harbin 150030, China*;
2. *Key Laboratory of Agricultural Renewable Resources Utilization Technology and Equipment in Cold Areas of Heilongjiang Province, Harbin 150030, China*)

Abstract: This study systematically investigated the evolution law of rheological properties in the anaerobic fermentation system of cow manure (CM) and corn straw (CS) mixtures at varying total solids (TS). Combined with computational fluid dynamics (CFD) simulations, the distribution characteristics of particles within fermentation system were revealed, illustrating the impact mechanisms of agitation strategies. Simulations demonstrated that higher agitation speeds and TS levels increase instantaneous power consumption while altering mixing and sedimentation dynamics. When TS was 6%, 120 r/min required more power than 100 r/min and 80 r/min, but 100 r/min reduced daily energy consumption by 4.30% and 3.19% compared to 80 r/min and 120 r/min. Under conditions of TS=6% and 8%, with maintained process stability, experimental groups increased energy output by 12.42% and 30.41% while reducing energy consumption by 13.60% and 3.39% versus control groups, demonstrating significant overall efficiency gains. Inversely, when TS was 10%, experimental groups decreased energy output by 0.34%, while increasing energy consumption. These findings prove that when TS is below 10%, optimized agitation strategies enable positive net energy output, establish an optimization scheme, and balance biogas production efficiency with economic feasibility.

Keywords: anaerobic digestion, rheological properties, agitation strategies, net energy

DOI: 10.25165/j.ijabe.20261903.10379

Citation: Liu Y Y N, Zhang K J, Sun Y. Net energy-oriented agitation optimization for cow manure–corn straw co-fermentation. Int J Agric & Biol Eng, 2026; 19(3): 281–293.

1 Introduction

Anaerobic fermentation is a highly efficient technology for treating organic waste and generating sustainable energy[1]. As biomass resources, straw and manure have the advantages of being renewable and having abundant reserves[2]. Anaerobic fermentation can effectively degrade manure and straw[3]. Co-digestion of straw and animal manure can reduce the C/N ratio and maintain nutritional balance[4]. To achieve thorough mixing of fermentation substrates and enhance gas production performance, adequate agitation of substrates within the reactor is essential[5]. Mechanical agitation provides higher shear forces that suppress scum layer formation and enhance mass and heat transfer. However, agitation energy consumption typically accounts for approximately 50% of the total energy consumption of biogas projects[6]. Thus, reducing agitation energy consumption while maintaining stable fermentation is critical for sustainable long-term operation. For existing biogas projects, reactor renovation entails high costs and requires extended validation periods to ensure system stability. Therefore, optimizing agitation strategies proves more effective in enhancing efficiency and productivity of biogas projects.

The CFD method enables optimization of equipment geometry by identifying vortices and dead zones, thereby reducing material inhomogeneity caused by dead zones and curbing energy losses induced by vortices[7,8]. The CFD method is further used to simulate flow field characteristics under diverse agitation strategies, capturing transient behaviors to assess impacts on mixing efficiency, shear stress, and energy consumption, thereby guiding strategy optimization[9]. Zhang et al.[10] employed CFD simulations to demonstrate significant alterations in flow fields and power consumption during mono-digestion of corn straw versus co-digestion with cow manure. At agitation speed of 80 r/min, power consumption exhibited a positive correlation with corn straw content in the fermentation broth. Research of Singh et al.[11] indicates that the optimal agitation strategy should first determine the minimum mixing requirements of the materials and equipment, and then achieve stable gas production and reduce energy consumption by shortening the agitation time and optimizing the intermittent cycle. Agitation enables uniform mixing, facilitating efficient contact between fermentation substrates and microorganisms[12]. Optimization of system-specific agitation strategies significantly enhances digestion efficiency and stability[13] by intensifying mass transfer[14], improving microbial habitats[15,16], preventing sludge sedimentation and crust formation, and enhancing gas release[17]. Ma et al.[18] conducted comparative trials during alkaline anaerobic sludge digestion involving continuous agitation (30 r/min, 90 r/min, 150 r/min) and 150 r/min intermittent agitation. Results demonstrated that the intermittent 150 r/min strategy elevated microbial abundance of unsaturated fatty acids and branched-chain fatty acids, potentially enhancing VFAs (volatile fatty acids) production while enriching *Firmicutes* and *Tissierella*. An optimal agitation strategy should minimize operational energy consumption while meeting fermentation requirements to maximize net energy output and enhance economic benefits of biogas projects.

Received date: 2025-12-12 **Accepted date:** 2026-06-03

Biographies: Yuyingnan Liu, PhD, research interest: anaerobic digestion, Email: tomtom12138@outlook.com; **Kejia Zhang**, MS, research interest: anaerobic digestion, Email: 13234661081@163.com.

***Corresponding author: Yong Sun**, PhD, Professor, research interest: anaerobic digestion. College of Engineering, Northeast Agricultural University, Harbin 150030, China. Tel: +86-13836145034, Email: sunyong@neau.edu.cn.

Li et al.[19] evaluated net energy output under varying agitation strategies (0, 2, 15, 30, 45 min/h and continuous agitation) during high-solid co-digestion of food waste and sludge. The 15 min/h strategy achieved peak net energy output (2.14×10^3 kW·h/t VS) and proved that agitation can effectively reduce system start-up time. It can be seen that research on agitation strategies is still relatively rare, and the formulation of agitation strategies still requires further study.

In response to the problems of low fermentation efficiency and high energy consumption resulting from poor mixing in co-fermentation systems of CM and CS, this study monitors feedstock rheological properties under varying TS. Through integrated CFD analysis, mass transfer efficiency within digesters under diverse agitation conditions is investigated. Based on these findings, optimized agitation strategies were formulated and the influence of agitation strategies on net energy output of the fermentation process was systematically evaluated to determine the optimal agitation strategy under varying TS.

2 Materials and methods

2.1 CFD simulation

2.1.1 Fermentation reactor structure

The fermentation reactor features an internal diameter of 130 mm, an effective height of 180 mm, and is equipped with a 65 mm diameter double-layer 45° pitched-blade turbine impeller. The physical modeling diagram of the fermentation reactor and system material distribution is shown in Figure 1a and Figure 1b.

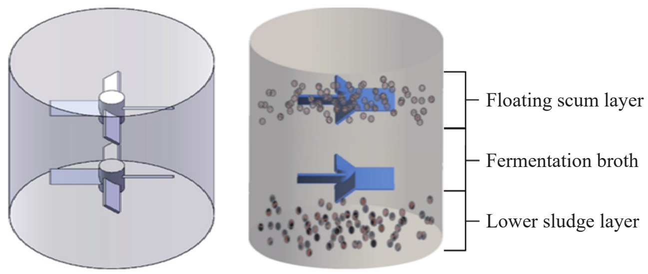

a. Physical modeling diagram of fermentation reactor b. System material distribution

Figure 1 System structure and material distribution diagram

2.1.2 Numerical simulation

This study consists of CM and CS particles and water. ANSYS FLUENT 2020 R1 (ANSYS, Inc., Pittsburgh, PA, USA) software was used for numerical simulation. The unstructured mesh was generated by ICEM 2020 R1 (ANSYS, Inc., Pittsburgh, PA, USA). The post-processing software was CFD-POST (ANSYS, Inc., Pittsburgh, PA, USA). Only granular phase and liquid phase were considered in this study. For simulating the co-digestion of CM and CS, the Eulerian-Eulerian multiphase flow model was selected to accurately capture interphase drag forces among scum layer, sludge layer, and fermentation broth. RNG (Re-Normalization Group) k-ε turbulence model was adopted due to the complex fluid interactions, multiphase flow dynamics, and high-fidelity requirements of this system.

2.1.3 Initial and boundary conditions

MRF (Multiple reference frame) method was employed to process rotation and stationary zones. The reactor bottom and walls were defined with no-slip boundary conditions to simulate realistic fluid-wall interactions. Pressure-velocity coupling utilized the SIMPLE (Semi-Implicit Method for Pressure-Linked Equations) algorithm, while discretization adopted the second-order upwind scheme with convergence residuals of 10^{-5} for all variables.

2.1.4 Grid independence

The computational domain was discretized using an unstructured hexahedral mesh. Following established methodology, mesh independence was verified via the Grid Convergence Index (GCI)[20]. Comparative analysis of three mesh resolutions (984,231, 1,568,648, and 2,073,372) yielded GCI values below 5% across all cases. Balancing computational economy and accuracy requirements, the optimal mesh number was determined to be 1,568,648.

2.2 Experimental materials

CS was air-dried naturally, crushed and sieved to a particle size of 3-5 mm, and stored in sealed containers under low-humidity conditions. Fresh CM was collected and sealed, then stored at −20°C for later use. Inoculum was taken from a biogas plant that had been operating continuously for more than one year (with corn stalks and cow manure as the substrates), then acclimated prior to experimental use. Material characteristics are listed in Table 1.

Table 1 Material characteristics

Index	Corn straw	Cow manure	Inoculum
TS/%	91.61±0.76	19.54±0.38	4.76±0.71
VS/%	83.56±0.29	17.25±1.04	3.17±0.82
C:N	57.67±2.46	17.25±1.78	16.19±0.19

2.3 Experiment setup

The co-fermentation substrate was prepared by mixing CM and CS at a 1:1 mass ratio with an inoculum-to-substrate ratio of 1:1, adjusting TS to 6%, 8%, and 10% respectively. Systems were operated at (35±1)°C with each hydraulic retention time (HRT) of 20 d and agitation speed at 60 r/min. A semi-continuous fermentation mode was employed. The apparent viscosity of scum and sludge layer was monitored, while the settling time of sludge particles under different TS was recorded. Building upon preliminary experimental data regarding viscosity variations and the thicknesses of both layers, numerical simulations were conducted to evaluate the mixing effectiveness under various agitation conditions (TS conditions of 6%, 8%, 10%, and agitation speeds of 80 r/min, 100 r/min, 120 r/min). These simulations yielded the agitation durations for each condition, enabling the calculation of respective energy consumption profiles. For semi-continuous validation, energy-optimized groups at each TS condition were comparatively evaluated against corresponding control reactors maintaining literature-standard parameters (60 r/min, 10 min continuous agitation, according to previous research). Finally, an economic analysis of the systems under different agitation strategies was performed by calculating the net energy output, which integrates both biogas production performance and energy consumption. Group settings for numerical simulation are listed in Table 2.

Table 2 Group settings for numerical simulation

Peer group	TS/%	Agitation speed/r·min^{-1}
T1	6	80
T2	6	100
T3	6	120
T4	8	80
T5	8	100
T6	8	120
T7	10	80
T8	10	100
T9	10	120

2.4 Analysis methods

TS and VS of samples were determined by the constant weight method[21]. pH was measured using a pH meter (PHSJ-4F, Shanghai Leici, China). VFAs were analyzed using a high-performance liquid chromatographer (Agilent 1290 infinity II, USA). Biogas compositions were analyzed using a gas chromatographer (Agilent GC7890, USA). All gas volumes were converted to the standard state (0°C and 101.3 kPa). Soluble chemical oxygen demand (sCOD) and ammonia nitrogen (AN) were analyzed using a multiparameter water quality analyzer (5B-6C, Beijing Lianhua, China). C/N was analyzed using an elemental analyzer (Euro Vector EA3000, Italy). Density was measured using a dual-purpose electronic densitometer (SJ-300GY, Shanghai Shuju, China). Apparent viscosity was measured using a rotational viscometer (NDJ-8S, Shanghai Lichen, China) at varying rotational speeds (6, 12, 30, 60 r/min). Mixing performance is comprehensively assessed based on the standard deviation formula of concentration distribution (which is indicated in Equation (1)), and agitation power (which is indicated in Equation (2)).

$$\sigma = \sqrt{1/n \sum_{i=1}^{n} (c_i/c_0 - 1)^2} \tag{1}$$

where, n is the number of sampling points; c_i is the solid particle volume fraction at sampling points; and c_0 is the mean solids particle volume fraction in the system.

$$PV = 2\pi MN/V \tag{2}$$

where, M is torque value, N·m; N is rotational speed, r/s; and V is total system volume, m^3.

Net energy output equation is indicated in Equation (3).

$$N = P(-) + E(+) \tag{3}$$

where, N is net energy output, kW·h; P is energy consumption, kW·h; and E is energy output, kW·h; Energy consumption is negative (−), while energy output is positive (+).

3 Results and discussion

3.1 Analysis of apparent viscosity

Previous studies have demonstrated that fermentation systems using livestock manure as substrate typically exhibit non-Newtonian fluid behavior[22,23]. This experiment monitored the apparent viscosity of the scum layer, sludge layer, and fermentation broth separately during the semi-continuous fermentation process, with viscosity measurements conducted after the settling phase concluded. The Herschel-Bulkley model is a classical model frequently employed to describe the rheological behavior of non-Newtonian fluids[24]. However, there still are certain limitations. As indicated by Equation (4), as γ approaches zero, the predicted viscosity tends towards infinity. This characteristic contradicts the actual properties of pseudoplastic fluids and compromises the accuracy of simulation outcomes. To mitigate this limitation, the measured apparent viscosity data were fitted using the power-law model which is shown in Equation (5). This model provides a more suitable and well-described representation of the rheological characteristics of materials involved in this study.

$$\eta = \tau/\gamma = \tau_y/\gamma + K(\gamma)^{n-1} \tag{4}$$

where, η is apparent viscosity, Pa·s; τ is shear stress, Pa; γ is shear rate, s^{-1}; τ_y is yield stress, Pa; K is consistency coefficient, Pa·s^n); and n is flow behavior index.

$$\ln\eta = (n-1)\ln 4\pi N + \ln K - n\ln n \tag{5}$$

where, N is rotational speed, r/min. When n<1, the fluid exhibits shear-thinning behavior; n=1, the fluid demonstrates Newtonian behavior; n>1, the fluid exhibits shear-thickening behavior. A higher K value indicates greater inherent viscosity of the fluid.

3.1.1 Apparent viscosity of fermentation broth

The results show that higher TS consistently corresponds to elevated overall apparent viscosity of the fermentation broth. Furthermore, all fermentation broths exhibited a characteristic pattern of initial viscosity increase followed by subsequent decrease during the first HRT (hydraulic retention time). As the fermentation progressed, the apparent viscosity stabilized with minor fluctuations during second and third HRT.

Under the TS condition of 6%, initial apparent viscosity of fermentation broth was 14.64 mPa·s. Subsequently, apparent viscosity gradually increased to the peak value of 34.26 mPa·s (6th day) and began to fluctuate and decrease after the 20th day. At this point, apparent viscosity was basically stable between 12.67 mPa·s and 17.65 mPa·s. For the TS condition of 8%, initial apparent viscosity was 32.29 mPa·s, and reached the peak value of 57.24 mPa·s on the 6th day; then apparent viscosity fluctuated and decreased, stabilizing at 32.56 mPa·s to 42.12 mPa·s. Under the TS condition of 10%, the initial value of apparent viscosity of fermentation broth was the highest among the three groups, which was 48.09 mPa·s; then it reached a peak of 86.76 mPa·s on the 10th day, and then fluctuated and decreased. After 20 d, it stabilized between 50.03 mPa·s and 60.98 mPa·s. It can be observed that a higher TS leads to a higher apparent viscosity peak, and apparent viscosity fluctuation range in the later stage of fermentation is relatively large and the decline trend is relatively slow. This may be related to the increase in the solid content in the fermentation broth caused by higher TS.

As N increases, η significantly decreases. When N is lower than 0.1 r/s, η is all higher than 339.8 mPa·s, which is inconsistent with the measured viscosity. It also reflects the limitations of the Herschel-Bulkley model. As N increases beyond 0.5 r/s, the non-Newtonian behavior of the fermentation broth progressively weakens while Newtonian behavior intensifies, causing the N-η curve to plateau. When N reaches 1.164 r/s, η stabilizes at 45.04 mPa·s, consistent with viscometer measurements. The variation of the apparent viscosity of the fermentation broth, the curve of the apparent viscosity of the fermentation broth varying with agitation speed, and the fitting curve of the power law model is shown in Figure 2a to Figure 2c.

3.1.2 Apparent viscosity of scum layer and sludge layer

Variations in apparent viscosity of both the scum and sludge layers with agitation speed, along with the corresponding power law model fitting results, are shown in Figure 3a to Figure 3d. All experimental groups exhibited consistent trends in apparent viscosity for both layers, and significant shear-thinning behavior was observed. For the scum layer, when N increased from 0.1 r/s to 1 r/s, when TS condition was 6%, η decreased from 1588.2 mPa·s to 198.6 mPa·s; when TS condition was 8%, η decreased from 2071.4 mPa·s to 274.4 mPa·s; when TS condition was 10%, η decreased sharply from 2422.6 mPa·s to 372.6 mPa·s. For the sludge layer, when N increased from 0.1 r/s to 1 r/s, when TS condition was 6%, η decreased from 758.2 mPa·s to 182.7 mPa·s; when TS was 8%, η decreased from 1377.5 mPa·s to 244.4 mPa·s; when TS condition was 10%, η decreased sharply from 1764.2 mPa·s to 386.5 mPa·s. As N increased from 0.1 to 1 r/s, the viscosity of both layers decreased markedly across all TS conditions. The n values of all the experimental groups were below unity (n<1), confirming the non-

Newtonian fluid characteristics of both layers. At identical TS, the scum layer consistently demonstrated higher apparent viscosity than the sludge layer. This phenomenon is ascribed to the composition of the scum layer, which is primarily dominated by CS particles resistant to degradation, where extensive microbial colonization occurs with substantial secretion of colloidal substances such as EPS. Conversely, the sludge layer consists mainly of organic particles from CM, microbial consortia, and metabolic byproducts. These components exhibit finer particle size, higher density, and enhanced tendencies for sedimentation and dispersion. The calculated n and K values are summarized in Table 3.

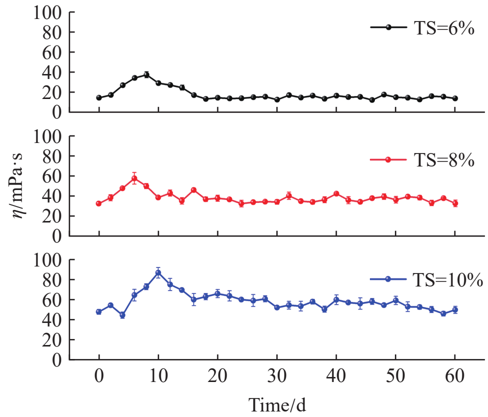

a. Apparent viscosity change of fermentation broth

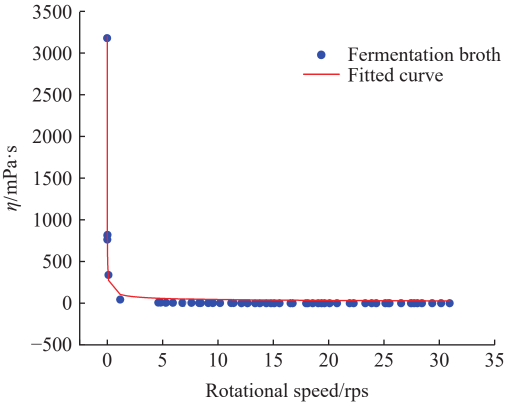

b. Apparent viscosity variation curve with agitation speed

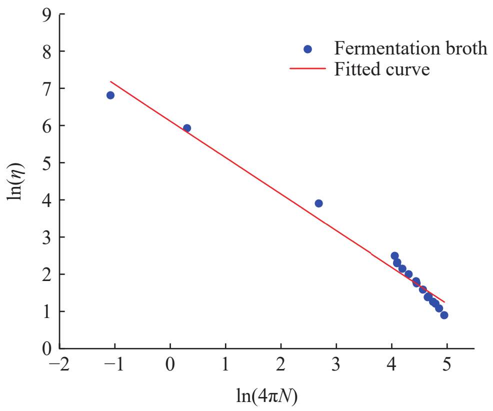

c. Power law model fitting curve

Figure 2 Apparent viscosity of fermentation broth varies with the agitation speed and fitting curve of the power law model

3.1.3 Particle settling characteristics

During the mid-to-late experimental phase, static sedimentation methodology was employed. Mixed materials from the reactor were transferred to beakers, homogenized thoroughly, and allowed to settle until complete stratification. The resulting sludge layer thicknesses for TS conditions of 6%, 8%, and 10% were measured as 39 mm, 52 mm, and 57 mm, respectively. Subsequently, the mixtures were re-homogenized and the time required to re-establish sedimentation to the marked thickness thresholds was recorded. Results demonstrated that the settling durations for TS conditions of 6%, 8%, and 10% were approximately 110 min, 210 min, and 270 min, respectively. These intervals were designated as the interval durations for subsequent agitation phases.

Table 3 n and K value of scum layer and sludge layer

	TS/%	n	K/Pa·s^n	R^2
Scum layer	6	0.108	1.55	0.996
	8	0.132	1.93	0.994
	10	0.182	2.05	0.992
Sludge layer	6	0.348	0.88	0.997
	8	0.286	1.62	0.994
	10	0.369	1.97	0.992

3.2 Evaluation of mixing performance based on CFD

3.2.1 Analysis of concentration distribution

Under different agitation speeds, the flow field distribution is roughly the same. The high-speed zone appears at the end of the impeller and generates a large shear rate at the end of the impeller. The fluid flows from the high-speed zone to the low-speed zone, resulting in the formation of vortices. The low-speed zone is distributed at the bottom of the reactor, on the wall surface and near the agitator shaft. When the agitation speed was low, the shear force and centrifugal force experienced by the part far from the impellers were small, and the *Re* value of the fluid was also small, making it less likely to move. As the agitation speed increased, the *Re* value of the fluid became larger, the resistance of the fluid to the impeller decreased, the ability of the impeller to drive the fluid movement enhanced, the flow velocity of solid particles significantly rose, the area of axial flow gradually expanded, and the uniformity of mixing also increased accordingly.

As agitation speed increased, the overall flow velocity of the fluid in the reactor also increased, and the dead zone area gradually decreased. When the agitation speed was 80 r/min, the flow velocity in most areas of the reactor was between 0.06 and 0.14 m/s, and the maximum speed was approximately 0.28 m/s. When the agitation speed was 100 r/min, the flow velocity in most areas of the reactor was between 0.09 and 0.17 m/s, and the maximum speed was approximately 0.35 m/s. When the agitation speed was 120 r/min, the flow velocity in most areas of the reactor was between 0.12 and 0.20 m/s, with a maximum speed of approximately 0.40 m/s. The velocity distribution was Z=90, Z=125, and Z=150 at different agitation speeds. It can be seen that the high-speed zone is located near the impellers, and the flow velocity gradually decreases along the radius. When the agitation speed was 80 r/min, the flow rate near the inner wall of the reactor was relatively low, and the uniformity of mixing was poor. As the agitation speed increased, the low-speed zone gradually decreased, which was more conducive to the mixing of materials. The particle velocity distribution in the reactor is shown in Figure 4a and Figure 4b.

When TS was 6%, as agitation progressed, scum layer particles migrated downward while sludge layer particles ascended upward. This flow pattern disrupted the initial stratification morphology, leading to diffusion to the position of the fermentation broth, ultimately achieving enhanced homogeneity. When TS was 8%, the

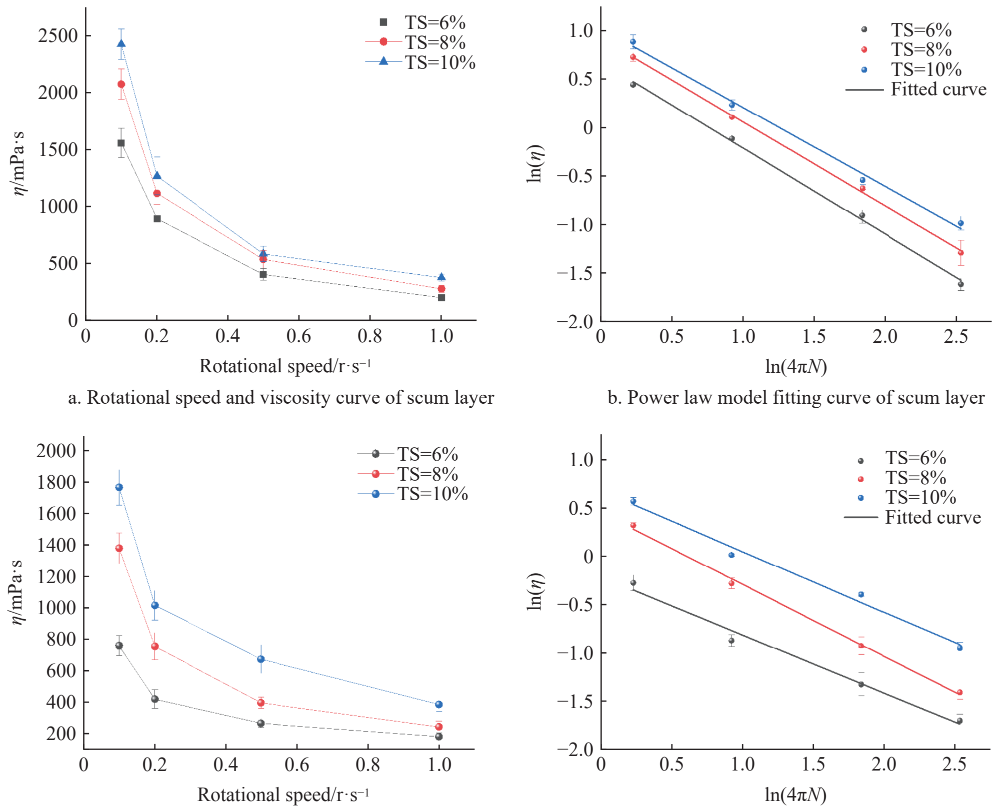

a. Rotational speed and viscosity curve of scum layer b. Power law model fitting curve of scum layer

c. Rotational speed and viscosity curve of sludge layer d. Power law model fitting curve of sludge layer

Figure 3 Apparent viscosity of scum and sludge layer varies with the agitation speed and fitting curve of the power law model

increase of agitation speed was conducive to the downward movement of scum layer particles and drove the upward movement of sludge layer particles, reducing the floating and sedimentation of particles.

Compared to TS conditions of 6% and 8%, the TS condition of 10% exhibits higher solids content, greater apparent viscosity in both scum and sludge layers, and increased mixing difficulty. Elevated agitation speeds enhance the dispersion capacity of the impeller, further preventing scum particles from aggregating upward and sludge particles from settling downward. The concentration distribution of scum and sludge layers under TS conditions of 6%, 8%, and 10% are shown in Figure 5a and Figure 5b.

The concentration deviations of scum particles and sludge particles along the Z-axis are shown in Figure 5c. At identical TS concentrations, σ of the sludge layer was approximately 1/3 to 1/2 that of the scum layer. This differential indicates that suspension performance of sludge layer particles is better, while the scum layer is more prone to aggregation. When TS was 6%, with the increasing of agitation speed from 80 to 120 r/min, σ presented a negligible increase from 0.1427 to 0.1431, while instantaneous power consumption rose significantly. When TS was 10%, the mean σ (0.09) was substantially lower than the TS condition of 6% (0.143). This demonstrates that higher TS levels amplify the positive impact of elevated agitation speeds on mixing homogeneity, potentially enhancing gas production efficiency.

3.2.2 Analysis of comprehensive energy consumption

Mixing completion was determined according to the international 95% criterion: When temporal fluctuations in solid-phase volume fraction remained within the 0%-5% range during continuous monitoring, the mixture was considered homogenized[25]. Concentration deviation varying with time is shown in Figure 6.

Three monitoring planes perpendicular to the Z-axis, which were designated as Z=30, Z=90, and Z=150, were established to evaluate mixing homogeneity. A system was deemed homogenized when the value of c/c_0 across these planes consistently resided within 0.95–1.05, indicating uniform solid particle distribution. Agitation duration under different operations is listed in Table 4.

Table 4 Agitation duration under different operations

Peer group	TS/%	Agitation speed/r·min⁻¹	Agitation duration/s
T1	6	80	310
T2	6	100	242
T3	6	120	202
T4	8	80	347
T5	8	100	274
T6	8	120	247
T7	10	80	472
T8	10	100	393
T9	10	120	314

Instantaneous power and energy consumption performance under different agitation strategies is shown in Table 5. The data indicate that higher TS necessitates greater agitation speeds, leading to elevated agitation power. At identical TS conditions, increased agitation speed raises agitation power but reduces agitation duration, ultimately lowering net energy consumption. For TS condition of 6%, T2 reduced energy consumption by 4.3% and 3.19%, compared to T1 and T3 respectively. For TS condition of 8%, T5 reduced energy consumption by 2.29% and 0.76%, compared to T4 and T6 respectively. Notably for TS condition of 10%, despite requiring the highest agitation speed, T9 achieved the lowest energy consumption as agitation duration was significantly shortened.

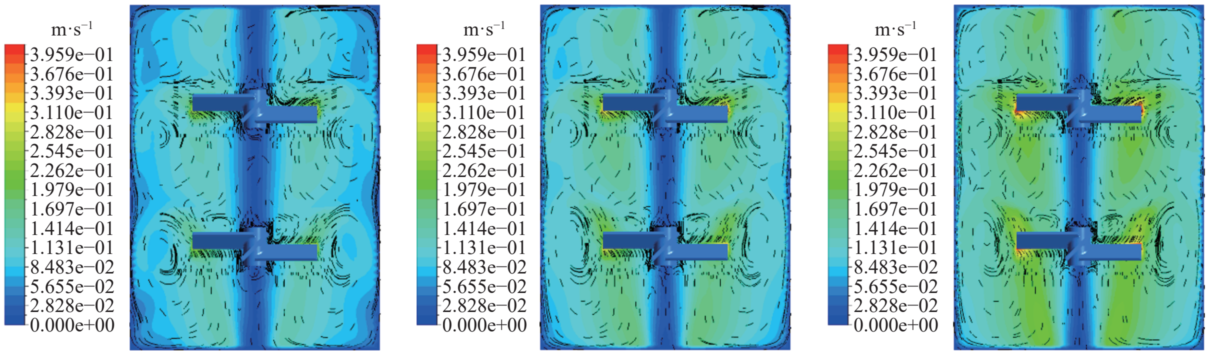

a. *X*-*Z*-axis plane velocity and streamlines

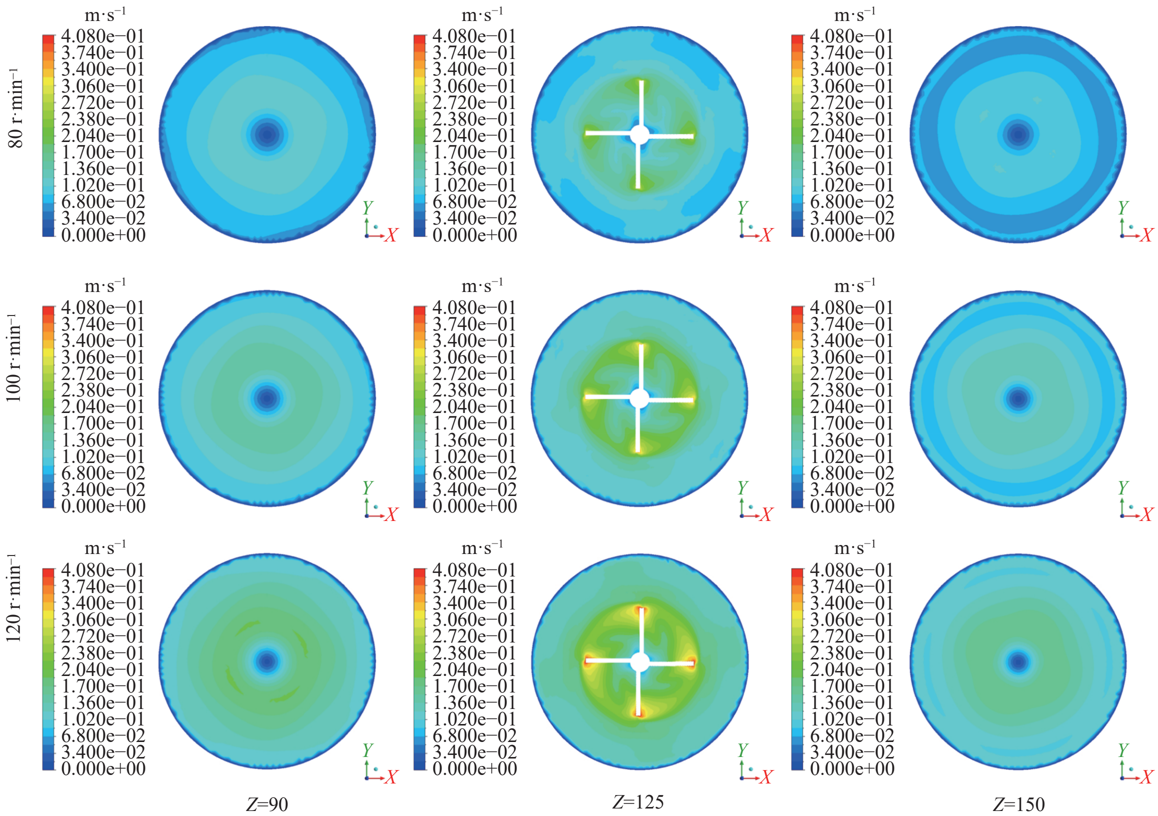

b. Velocity distribution in *Z*=90, 125, 150 planes at different agitation speeds

Figure 4 Particle velocities on different sections

Table 5 Instantaneous power and energy consumption under different operations

Peer group	Average power/W	Agitation duration/min	Interval duration/min	Energy consumption/kW·h·d⁻¹
T1	5.61	5.17	110	0.031 44
T2	6.39	4.03	110	0.030 17
T3	7.08	3.37	110	0.031 15
T4	7.74	5.78	220	0.032 16
T5	8.47	4.57	220	0.031 45
T6	9.30	4.17	220	0.031 78
T7	8.80	7.87	270	0.034 95
T8	12.15	6.55	270	0.034 87
T9	13.91	5.17	270	0.033 84

3.3 Analysis of fermentation characteristics

Prior to semi-continuous experimentation, batch tests were initially conducted using strategies T1, T2, and T3. CK group operations maintained identical TS with agitation speed of 60 r/min, 10-minute agitation duration, and 110 min interval duration. Under standard conditions, 1 m^3 of methane generates 1.6-2.4 kW·h of electricity[26]. Taking 2.0 kW·h/m^3 as the calculation standard, results demonstrate that agitation energy consumption exerts a more pronounced impact on overall economic performance than biogas output variations under comparable biogas production levels. Net energy accounting is listed in Table 6.

Table 6 Net energy accounting in batch tests

Peer group	CK	T1	T2	T3
Average power/(10^{-3} kW)	4.488	5.609	6.385	7.081
Cumulative gas production/L	17.347	15.726	17.174	16.167
Energy output/kW·h	+0.0347	+0.0315	+0.0343	+0.0323
Energy consumption/kW·h	−1.1612	−1.1004	−1.0559	−1.0903
Net energy output/kW·h	−1.1265	−1.0689	−1.0216	−1.058

Based on this conclusion, experimental groups selected through this screening process were designated as group S4, S5, and S6, and corresponding control groups were designated as group S1, S2, and S3 respectively. The detailed experimental design is comprehensively presented in Table 7.

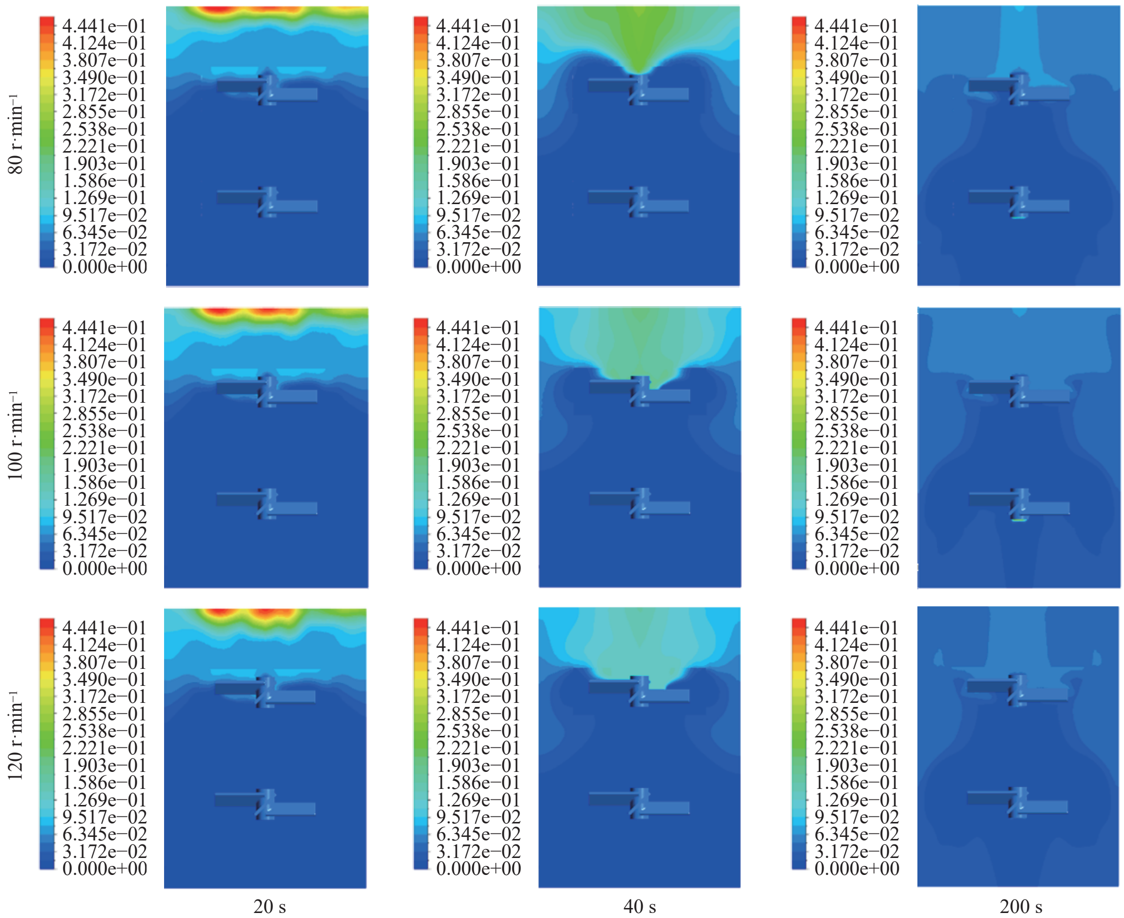
80 r·min⁻¹
100 r·min⁻¹
120 r·min⁻¹
4.441e−01
4.124e−01
3.807e−01
3.490e−01
3.172e−01
2.855e−01
2.538e−01
2.221e−01
1.903e−01
1.586e−01
1.269e−01
9.517e−02
6.345e−02
3.172e−02
0.000e+00
20 s
40 s
200 s

TS=6%

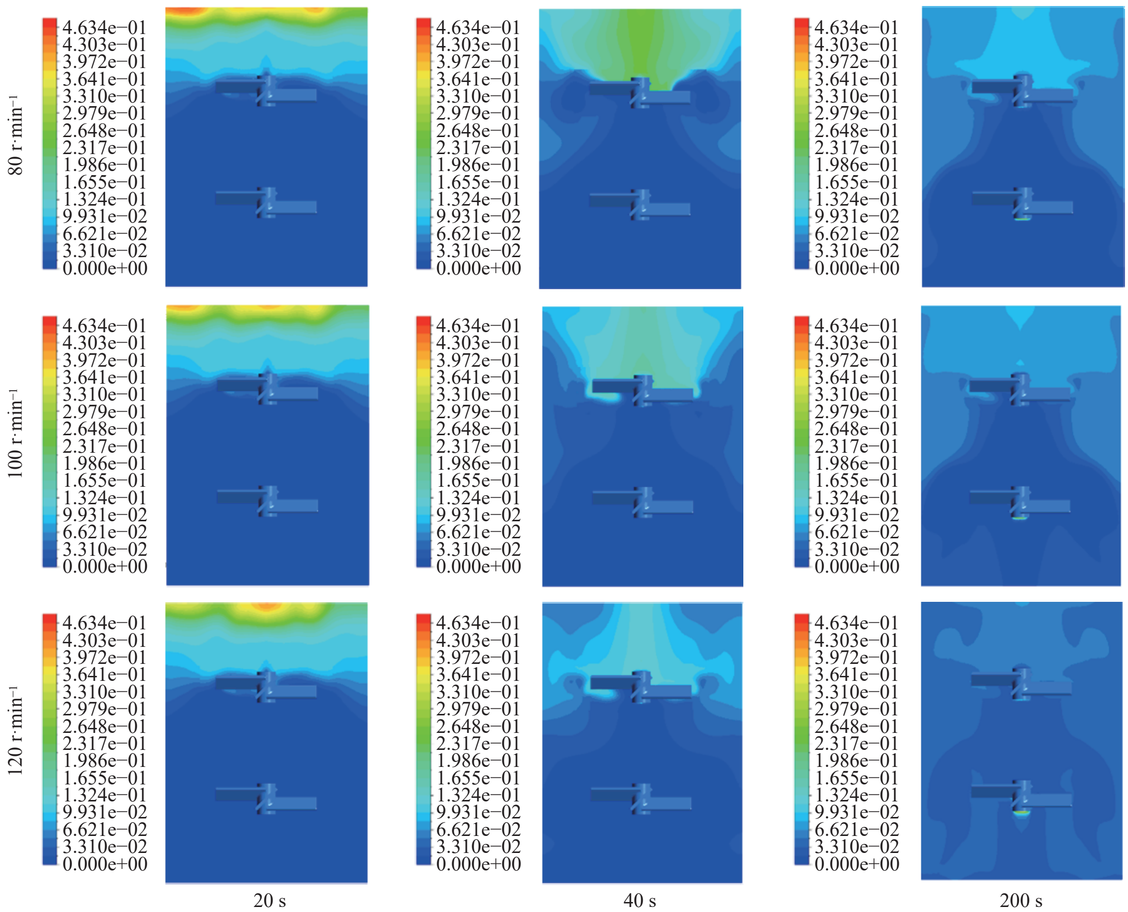
80 r·min⁻¹
100 r·min⁻¹
120 r·min⁻¹
4.634e−01
4.303e−01
3.972e−01
3.641e−01
3.310e−01
2.979e−01
2.648e−01
2.317e−01
1.986e−01
1.655e−01
1.324e−01
9.931e−02
6.621e−02
3.310e−02
0.000e+00
20 s
40 s
200 s

TS=8%

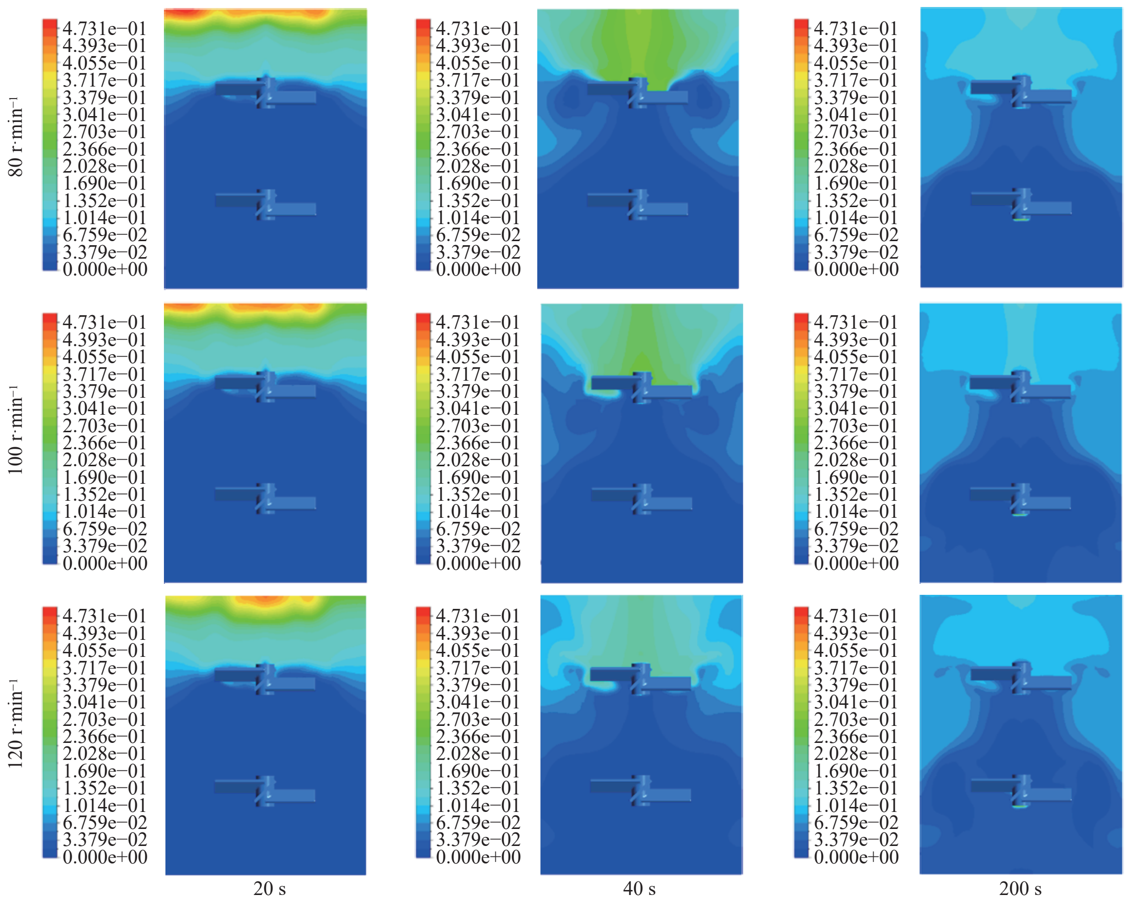

TS=10%

a. Concentration distribution of scum layer varies with time at different agitation speeds under different TS

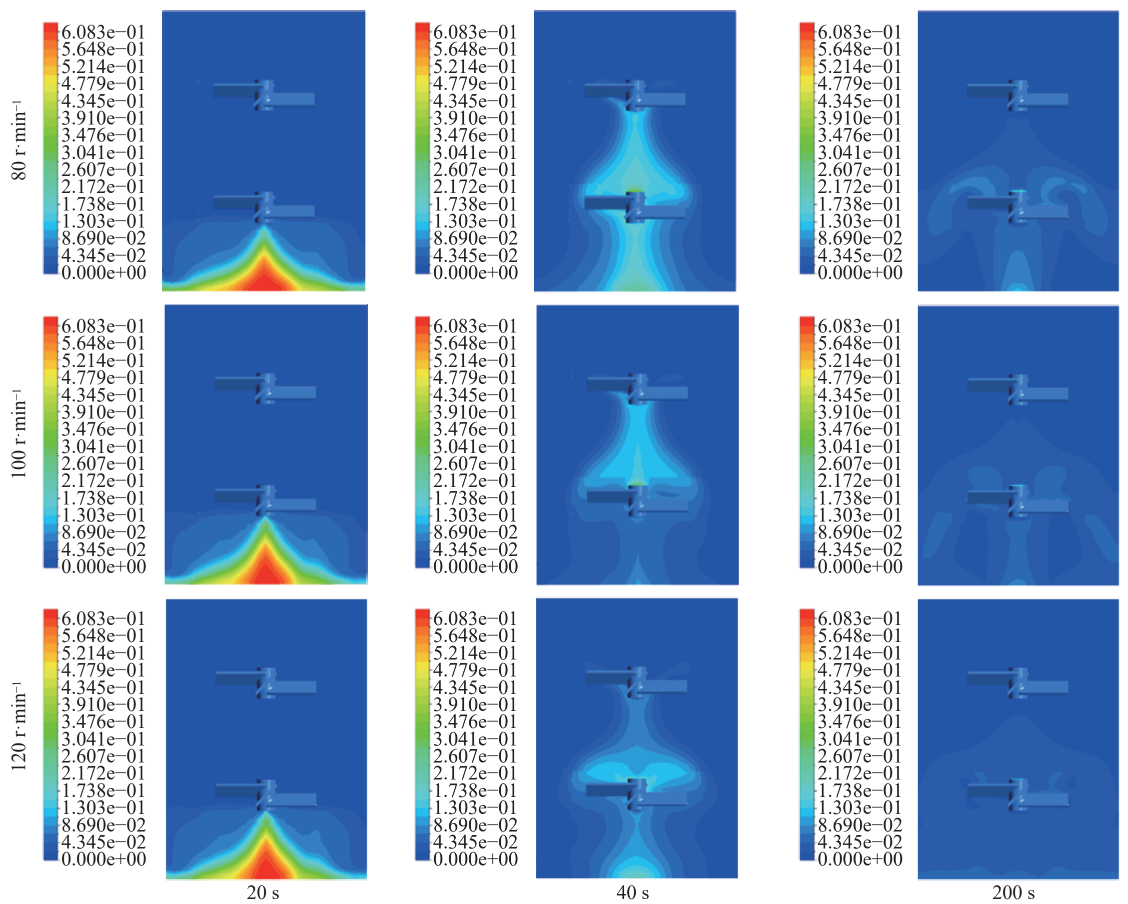

TS=6%

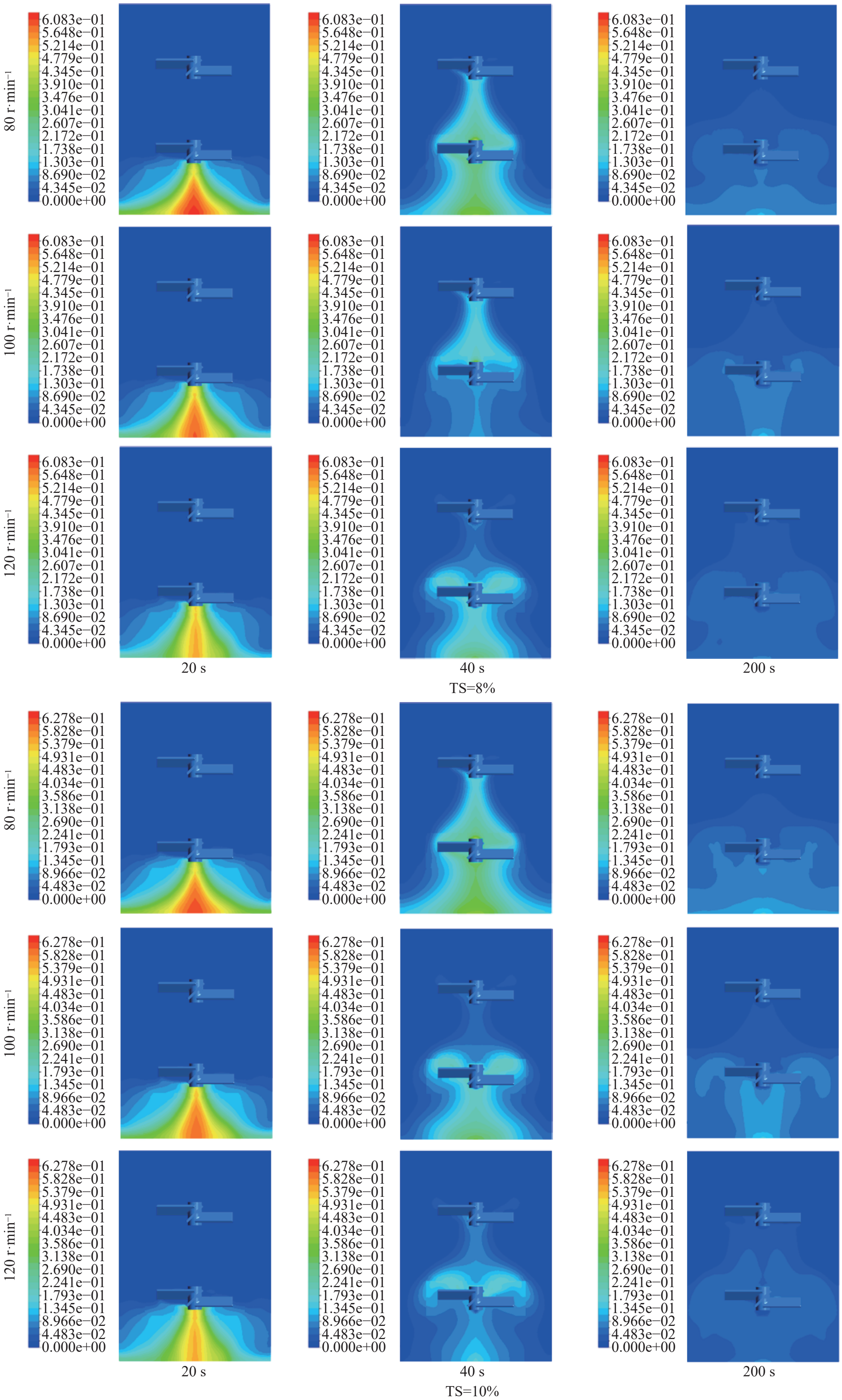

b. Concentration distribution of sludge layer varies with time at different agitation speeds under different TS

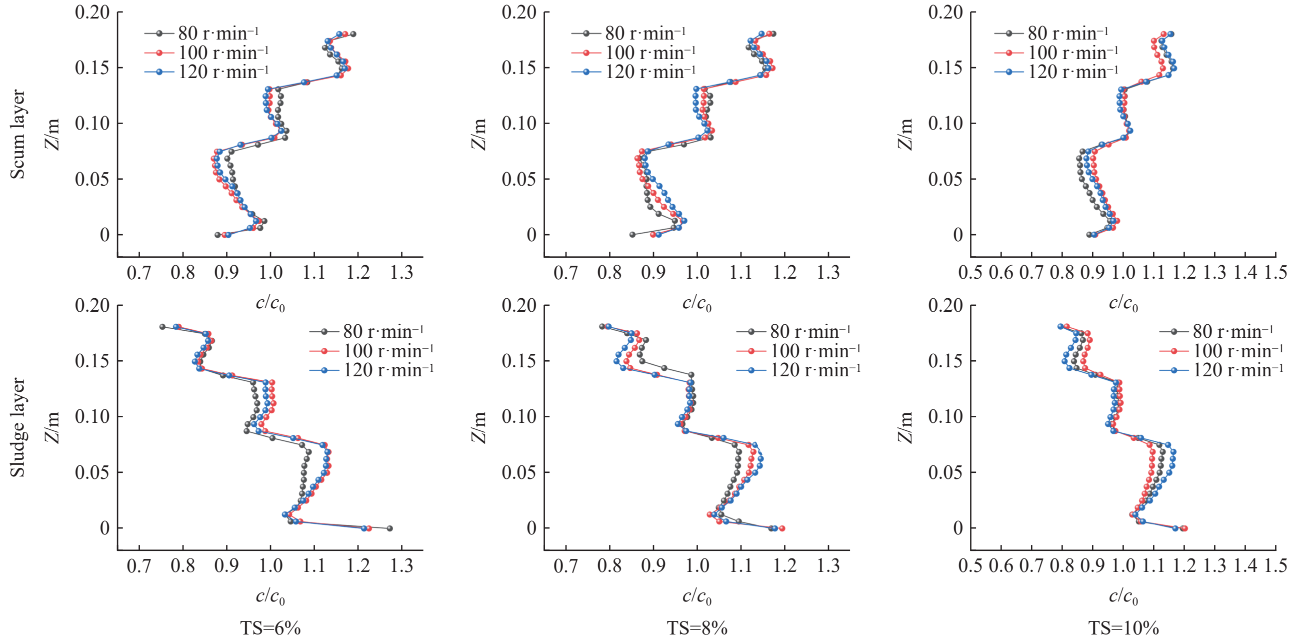

c. Concentration deviation curve along Z-axis

Figure 5 Concentration changes of scum layer and sludge layer

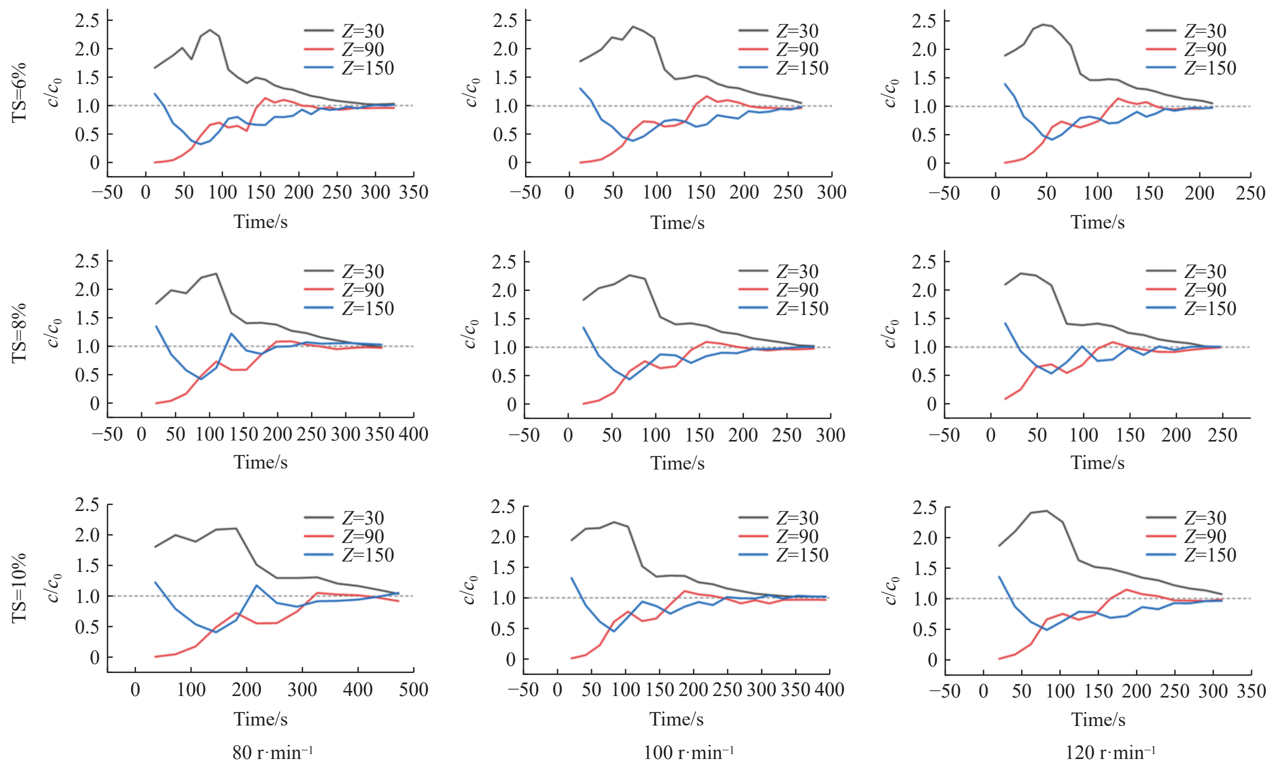

Figure 6 Concentration deviation varies with time

Table 7 Semi-continuous experimental groups

Peer group	TS /%	Agitation speed /r·min^{-1}	Agitation duration /min	Interval duration /min
S1	6	60	10	110
S2	8	60	10	220
S3	10	60	10	270
S4	6	100	4.03	110
S5	8	100	4.57	220
S6	10	120	5.17	270

3.3.1 Analysis of gas production characteristics

Gas production characteristics across experimental groups are shown in Figure 7. Volumetric daily biogas yields in S2 to S6 demonstrated an initial increase followed by stabilization, whereas S1 exhibited no distinct production peak. This divergence likely stems from early-stage scum layer formation due to low-density straw flotation at 60 r/min (insufficient for scum disruption), while S4 elevated agitation at 100 r/min, effectively fracturing the scum layer and enhancing fermentation efficiency.

Regarding the volumetric gas production rate, when TS was 6%, S4 reached 665.5 mL/L·d, achieving 23.03% higher average daily biogas yields than S1, which was 540.9 mL/L·d. When TS was 8%, S5 reached 1003.2 mL/L·d, surpassing S2 by 39.63%, which is 718.4 mL/L·d. Notably, when TS was 10%, the volumetric gas production rate showed limited enhancement; S6 reached 1138.1 mL/L·d, surpassing S3 by only 0.33%, which was 1141.9 mL/L·d. Regarding the methane production rate, when TS was 6%, S4 reached 54.39%, reaching a 4.12% higher methane content than S1, which was 52.24%. When TS was 8%, S5 reached 55.57%, reaching a 3.41% higher methane content than S2, which was 53.74%. When TS was 10%, S6 reached 54.44%, and S3 reached 54.06%, which were comparable.

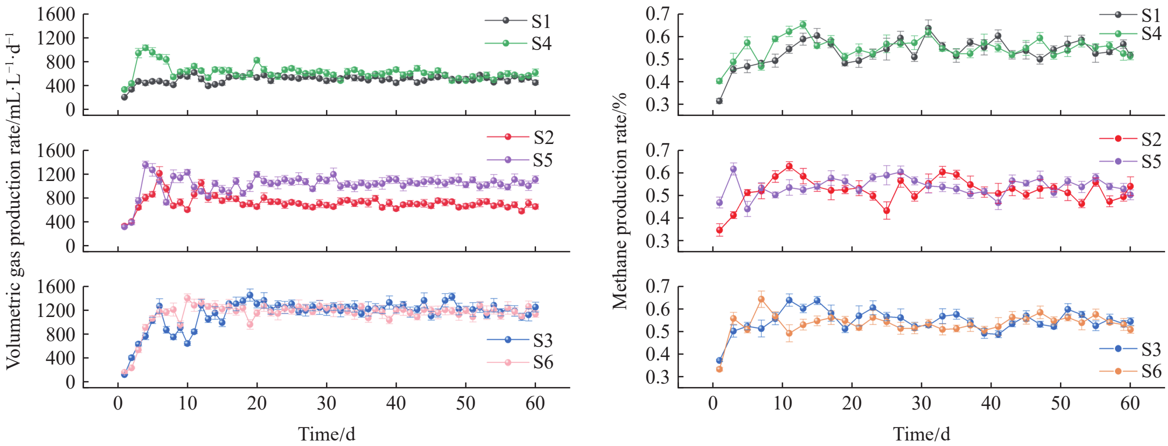

Figure 7 Gas production characteristics

Early gas production limitations may derive from suboptimal fluidity restricting microbial-substrate contact, where low agitation speeds induced localized VFAs accumulation, constraining gas production. The subsequent enhancement in biogas production may be attributed to improved mass transfer from rheological modification, coupled with microbial adaptation to shear forces. Microbial community maintains structural integrity while promoting more complete substrate degradation.

Results indicated that optimized agitation strategies did not compromise system stability. Moreover, with low TS conditions, it can even lead to an increase in stability, which is manifested as an improvement in gas production.

3.3.2 Analysis of system stability

Fermentation stability was assessed via key indicators, which are pH, TAN (total ammonia nitrogen), sCOD, and VFAs, with variation trends shown in Figure 8.

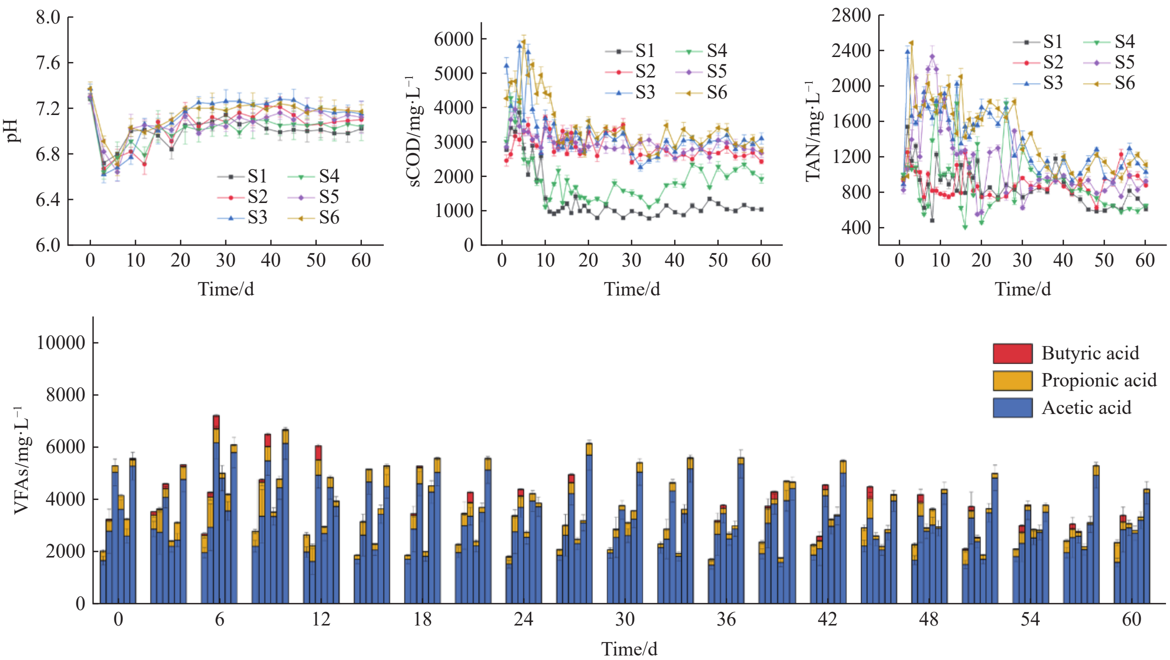

Figure 8 Variations of pH, sCOD, TAN, and VFAs

It can be seen that pH of all groups exhibited an initial significant decline followed by gradual recovery. The lowest pH level was achieved at 3-6 d, and then gradually increased until the twentieth day and remained stable, indicating that microorganisms gradually adapted to the environment, metabolic activities tended to balance, and the production and consumption of organic acids reached a dynamic equilibrium. Stabilized pH increased with TS, reaching 7.2 at the TS condition of 10%, which exceeded levels at TS conditions of 6% and 8%. This is likely due to ammonia accumulation neutralizing H^+ ions. Optimized strategies demonstrated greater pH stability than controls throughout fermentation. In terms of stability, the pH fluctuations in each experimental group showed a more stable trend compared to the control group.

TAN concentrations exhibited elevated and volatile levels across all groups during the initial 30 d. The average TAN of S1 to

S6 in the first 30 d were 959.36 mg/L, 928 mg/L, 1537.87 mg/L, 997.06 mg/L, 1283.3 mg/L, and 1653.26 mg/L, respectively. With the fermentation reaction proceeding, TAN levels gradually declined and stabilized across all groups as the reaction progressed. The TAN levels with TS conditions of 6%, 8%, and 10% fluctuated around 620 mg/L, 810 mg/L, and 1000 mg/L respectively. The modification of agitation strategies demonstrated negligible impact on TAN, confirming that agitation strategies do not compromise fermentation stability.

It can be seen that sCOD level of the system is positively correlated with the TS of the system. The mean sCOD at TS condition of 10% reached 3401.98 mg/L, exceeding TS conditions of 6% and 8% by 13.92% and 49.91%, which were 1704.13 mg/L and 2928.36 mg/L, respectively. The sCOD peak values in each group in the early stage all occurred around the fifth day. The sCOD peak values of S1 to S6 were 3852 mg/L, 3702 mg/L, 5778 mg/L, 4274 mg/L, 3942 mg/L, and 5904 mg/L, respectively. As the fermentation reaction proceeded, the value of sCOD gradually decreased. Agitation strategy modifications universally elevated sCOD concentrations, thereby facilitating microbial growth, proliferation, and metabolic activity to enhance fermentation efficiency.

The VFAs levels in each experimental group showed an upward trend in the first 9 d and then gradually stabilized. The VFAs levels in S1 and S4 remained at 2400-3500 mg/L after the first HRT. The total volatile acid concentrations in S2 and S5 were between 2800-4500 mg/L, and those in S3 and S6 were mostly between 3900-5800 mg/L. Research indicates that elevated VFAs levels enhance process stability, but concentrations exceeding 6,000 mg/L inhibit anaerobic digestion[27]. Group S3 surpassed this threshold on days 6, 9, and 12, whereas S6 exhibited no such situations. The gas production of the fermentation system was inhibited during this period, which is consistent with the situation of gas production. This might be due to the excessively high TS conditions of the system, and the agitation speed of 60 r/min was difficult to evenly distribute the materials, resulting in the accumulation of VFAs. Optimized groups consistently maintained higher VFAs than controls without exceeding the inhibitory limit, confirming enhanced process stability under optimized strategies. Notably, as a critical methanogenic intermediate, acetic acid demonstrated elevated levels in optimized groups, suggesting improved biogas potential. This enhancement likely stems from superior mixing homogeneity resulting from changes of agitation strategies, which promotes VFAs generation while mitigating spatial heterogeneity in VFAs distribution.

3.4 Economic analysis of fermentation

Energy consumption and output across fermentation systems under different agitation strategies is listed in Table 8. For TS=6%, S4 achieved 12.42% higher energy output than S1 while reducing energy consumption by 13.60%. At TS=8%, S5 increased energy output by 30.41% with a 3.39% reduction in consumption compared to S2. Conversely, at TS=10%, S6 exhibited a 0.34% decrease in energy output and a 0.0948 kW·h increase in consumption compared to S3. These results demonstrate that optimized agitation strategies enhance apparent efficacy at lower TS levels, but economic viability diminishes at high TS due to disproportionately high energy input for agitation.

Table 8 Net energy accounting with different agitation strategies

Peer group	S1	S2	S3	S4	S5	S6
Average power/(10^{-3} kW)	4.488	5.512	6.013	6.39	8.47	13.91
Gas production/L	45.44	56.03	89.065	51.909	79.767	88.77
Energy output/kW·h	+0.0909	+0.1121	+0.1781	+0.1038	+0.1595	+0.1775
Energy consumption/kW·h	−1.992	−1.8602	−1.8355	−1.7211	−1.7971	−1.9303
Net energy output/kW·h	−1.9011	−1.7481	−1.6574	−1.6173	−1.6376	−1.7528

4 Conclusions

In CM and CS co-fermentation, the scum layer exhibits higher non-Newtonian properties than the sludge layer. Simulation analysis indicates that higher TS requires more agitation speed but reduces energy consumption due to shortened agitation duration. Semi-continuous experiments showed that agitation strategies enhanced biogas production at TS=6% and 8%, but this was not obvious at 10%. Overall, system stability demonstrated universal enhancement. Economic analysis revealed that S5 yielded optimal benefits compared with S2, and S6 decreased net energy due to high agitation energy despite similar gas production. In conclusion, agitation strategy provides net energy gains at TS<10%, while high-TS systems require balancing biogas potential against energy costs.

Acknowledgements

This work was supported by the National Natural Science Foundation of China (Grant No. 52476182) and the Heilongjiang Spring Goose Program for Innovative Talents (Grant No. CYCX24005).

[References]

[1] Chen X T, Cui Z J, Zhao Y H, Zhu N, Liu Y, Hu Z H, et al. Synergistic mechanism of substrate hydrolysis and methanogenesis under "gradient anaerobic digestion" process. Energy Conversion and Management, 2024; 309: 118443.

[2] Tsafrakidou P, Bekatorou A, Koutinas A A, Kordulis C, Banat I M, Petsi T, et al. Acidogenic fermentation of wheat straw after chemical and microbial pretreatment for biofuel applications. Energy Conversion and Management, 2018; 160: 509–517.

[3] Wang X G, Liu T Q, Liu Y Y N, Sun Y. Effects of stirring time on anaerobic digestion of cattle manure-corn stover: Microbial diversity and metabolic pathways. Fuel, 2024; 367: 131468.

[4] Meng X H, Zhen F, Yang J C, Zhang Q G, Zhang Z Y, Qu B, et al. A multistage biogas slurry reflux and spray anaerobic digestion reactor for high solid anaerobic digestion: Performance and application evaluation. Energy Conversion and Management, 2024; 321: 119060.

[5] Liu D, Cen R X, Yuan A, Wu M X, Luo C, Chen M M, et al. Effects of continuous low-speed biogas agitation on anaerobic digestion of high-solids pig manure: Performance and microbial community. Journal of Environmental Management, 2024; 354: 120355.

[6] Michelan R, Zimmer T R, Rodrigues J A D, Ratusznei S M, de Moraes D, Zaiat M, et al. Effect of impeller type and mechanical agitation on the mass transfer and power consumption aspects of ASBR operation treating synthetic wastewater. Journal of Environmental Management, 2009; 90(3): 1357–1364.

[7] Alobaid F, Almohammed N, Massoudi Farid M, May J, Rößger P, Richter A, et al. Progress in CFD simulations of fluidized beds for chemical and energy process engineering. Progress in Energy and Combustion Science, 2022; 91: 100930.

[8] Pakzad L, Ein-Mozaffari F, Upreti S R, Lohi A. Evaluation of the mixing of non-Newtonian biopolymer solutions in the reactors equipped with the coaxial mixers through tomography and CFD. Chemical Engineering Journal, 2013; 215-216: 279–296.

[9] Cheng J P, Wu S, Wang X F, Shi Y F, Guo J B, Qiao N, et al. The dispersion of Trichosporon fermentans was controlled by optimizing the shear environment in the reactor to improve the cell sedimentation and separation performance. Journal of Cleaner Production, 2023; 414: 137649.

[10] Zhang Y, Yu G R, Yu L, Siddhu M A H, Gao M J, Abdeltawab A A, et al. Computational fluid dynamics study on mixing mode and power consumption in anaerobic mono- and co-digestion. Bioresource Technology, 2016; 203: 166–172.

[11] Singh B, Szamosi Z, Siménfalvi Z. Impact of mixing intensity and duration on biogas production in an anaerobic digester: a review. Critical Reviews in Biotechnology, 2020; 40(4): 508–521.
[12] Rocamora I, Wagland S T, Villa R, Simpson E W, Fernández O, Bajón-Fernández Y. Dry anaerobic digestion of organic waste: A review of operational parameters and their impact on process performance. Bioresource Technology, 2020; 299: 122681.
[13] Dai X H, Hua Y, Li H P, Liu R, Chen S X, Dai L L, et al. Coupling self-sustaining air flotation screening with conventional CSTR enhances anaerobic biodegradability of corn stover. Bioresource Technology, 2020; 310: 123417.
[14] Kress P, Nägele H-J, Oechsner H, Ruile S. Effect of agitation time on nutrient distribution in full-scale CSTR biogas digesters. Bioresource Technology, 2018; 247: 1–6.
[15] Kariyama I D, Zhai X D, Wu B X. Influence of mixing on anaerobic digestion efficiency in stirred tank digesters: A review. Water Research, 2018; 143: 503–517.
[16] Lindmark J, Eriksson P, Thorin E. The effects of different mixing intensities during anaerobic digestion of the organic fraction of municipal solid waste. Waste Management, 2014; 34(8): 1391–1397.
[17] Latha K, Velraj R, Shanmugam P, Sivanesan S. Mixing strategies of high solids anaerobic co-digestion using food waste with sewage sludge for enhanced biogas production. Journal of Cleaner Production, 2019; 210: 388–400.
[18] Ma S J, Xu K, Ren H Q. Effect of mixing intensity on volatile fatty acids production in sludge alkaline fermentation: Insights from dissolved organic matter characteristics and functional microorganisms. Journal of Environmental Management, 2023; 345: 118801.
[19] Li L L, Gao Q W, Wang K, Zhao Q L, Zhou H M, Jiang J Q, et al. Intermittent mixing facilitates energy recovery and low carbon emissions from high-solids anaerobic co-digestion of food waste and sewage sludge. Environmental Technology & Innovation, 2023; 32: 103339.
[20] Kelly W, Gigas B. Using CFD to predict the behavior of power law fluids near axial-flow impellers operating in the transitional flow regime. Chemical Engineering Science, 2003; 58(10): 2141–2152.
[21] Liu Y Y N, Wang X G, Sun Y. Optimization and experimental study of variable frequency intermittent stirring strategy for anaerobic digestion based on CFD. Fuel, 2024; 355: 129371.
[22] Hreiz R, Adouani N, Fünfschilling D, Marchal P, Pons M-N. Rheological characterization of raw and anaerobically digested cow slurry. Chemical Engineering Research and Design, 2017; 119: 47–57.
[23] Wei L L, Ren Y M, Zhu F Y, Xia X H, Xue C H, Yang H Z, et al. Horizontal flow reactor optimization for biogas recovery during high solid organics fermentation: Rheological characteristic analyses. Journal of Water Process Engineering, 2021; 40: 101776.
[24] Dai X H, Gai X, Dong B. Rheology evolution of sludge through high-solid anaerobic digestion. Bioresource Technology, 2014; 174: 6–10.
[25] Yao Q W, Yang K, Zhang X X, Yin W L, Pan J X, Wang H, et al. Evaluation on the mixing state of solid-liquid two-phase in stirred tank via an improved Voronoi diagram approach. Powder Technology, 2025; 453: 120620.
[26] Wu Y Y, Chang X N, Zhang J W. Environmental emission evaluation for straw biogas power generation and bio-natural gas preparation based on LCA method. China Biogas, 2020; 38(01): 59–65. (in Chinese)
[27] Siegert I, Banks C. The effect of volatile fatty acid additions on the anaerobic digestion of cellulose and glucose in batch reactors. Process Biochemistry, 2005; 40(11): 3412–3418.